Ho:YAG single crystal fiber: fabrication and optical characterization

Yuan Li,[1] Eric G. Johnson,[1,*] Craig D. Nie,[2] James A. Harrington,[2] and Ramesh Shori[3]

[1]*The Holcombe Department of Electrical and Computer Engineering, Center for Optical Materials Science and Engineering Technologies (COMSET), Clemson University, Clemson, South Carolina 29634, USA*
[2]*Department of Material Science and Engineering, Rutgers University, Piscataway, NJ 08854, USA*
[3]*SPAWAR System Center, Advanced Concepts Group, San Diego, CA 92152 USA*
[*]*ejohns8@clemson.edu*

Abstract: 0.5% Holmium (Ho) doped YAG single crystal fiber (SCF) was fabricated using Laser Heated Pedestal Growth (LHPG) method and characterized for its optical absorption and emission properties involving transitions between the $^5I_8$ and $^5I_7$ energy levels. The results verified the absorption peaks suitable for in-band direct pumping at 1908 nm and 1932 nm with the emission occurring between 2050 and 2150 nm. Small signal gain measurements were also performed for demonstrating the fiber like characteristics of the SCF.

OCIS codes: (160.5690) Rare-earth-doped materials; (160.3380) Laser materials; (060.2290) Fiber materials.

References and links

1. X. Délen, S. Piehler, J. Didierjean, N. Aubry, A. Voss, M. A. Ahmed, T. Graf, F. Balembois, and P. Georges, "250 W single-crystal fiber Yb:YAG laser," Opt. Lett. **37**(14), 2898–2900 (2012).
2. N. Ter-Gabrielyan, V. Fromzel, X. Mu, H. Meissner, and M. Dubinskii, "High efficiency, resonantly diode pumped, double-clad, Er:YAG-core, waveguide laser," Opt. Express **20**(23), 25554–25561 (2012).
3. X. Délen, I. Martial, J. Didierjean, N. Aubry, D. Sangla, F. Balembois, and P. Georges, "34 W continuous wave Nd:YAG single crystal fiber laser emitting at 946 nm," Appl. Phys. B **104**(1), 1–4 (2011).
4. P. C. Shi, I. A. Watson, and J. H. Sharp, "High-concentration Er:YAG single-crystal fibers grown by laser-heated pedestal growth technique," Opt. Lett. **36**(12), 2182–2184 (2011).
5. X. Délen, Y. Zaouter, I. Martial, N. Aubry, J. Didierjean, C. Hönninger, E. Mottay, F. Balembois, and P. Georges, "Yb:YAG single crystal fiber power amplifier for femtosecond sources," Opt. Lett. **38**(2), 109–111 (2013).
6. W. X. Zhang, J. Zhou, W. B. Liu, J. Li, L. Wang, B. X. Jiang, Y. B. Pan, X. J. Cheng, and J. Q. Xu, "Fabrication, properties and laser performance of Ho:YAG transparent ceramic," J. Alloy. Comp. **506**(2), 745–748 (2010).
7. J. S. Haggerty, W. P. Menashi, and J. F. Wenekkus, "Method for forming refractory fibers by laser energy," US Patent 3944640 (1976).
8. D. H. Jundt, M. M. Fejer, and R. L. Byer, "Characterization of single-crystal sapphire fibers for optical power delivery systems," Appl. Phys. Lett. **55**(21), 2170–2172 (1989).
9. R. S. Feigelson, "Pulling optical fibers," J. Cryst. Growth **79**(1-3), 669–680 (1986).
10. R. S. F. Chang, S. Sengupta, L. B. Shaw, and N. Djeu, "Fabrication of laser materials by laser-heated pedestal growth," Proc. SPIE **1410**, 125–132 (1991).
11. R. K. Nubling and J. A. Harrington, "Optical properties of single-crystal sapphire fibers," Appl. Opt. **36**(24), 5934–5940 (1997).
12. http://www.crystran.co.uk/
13. K. Y. Huang, K. Y. Hsu, D. Y. Jheng, W. J. Zhuo, P. Y. Chen, P. S. Yeh, and S. L. Huang, "Low-loss propagation in Cr4+:YAG double-clad crystal fiber fabricated by sapphire tube assisted CDLHPG technique," Opt. Express **16**(16), 12264–12271 (2008).
14. M. J. F. Digonnet, C. J. Gaeta, D. O'Meara, and H. J. Shaw, "Clad Nd:YAG fibers for laser applications," J. Lightwave Technol. **5**(5), 642–646 (1987).
15. S. A. Payne, L. L. Chase, L. K. Smith, W. L. Kway, and W. F. Krupke, "Infrared cross-section measurements for crystals doped with Er3+, Tm3+, and Ho3+," IEEE J. Quantum Electron. **28**(11), 2619–2630 (1992).
16. G. A. Kumar, M. Pokhrel, D. K. Sardar, P. Samuel, K. I. Ueda, T. Yanagitani, and H. Yagi, "2.1 μm emission spectral properties of Tm and Ho doped transparent YAG ceramic," Sci. Adv. Mater. **4**(5), 617–622 (2012).
17. D. C. Brown, V. Envid, and J. Zembek, "Ho:YAG absorption cross sections from 1700 to 2200 nm at 83, 175, and 295 K," Appl. Opt. **51**(34), 8147–8158 (2012).

#209986 - $15.00 USD Received 11 Apr 2014; revised 3 Jun 2014; accepted 4 Jun 2014; published 10 Jun 2014

18. Q. Dong, G. Zhao, J. Chen, Y. Ding, and C. Zhao, "Growth and anisotropic thermal properties of biaxial Ho:YAlO3 crystal," J. Appl. Phys. **108**(2), 023108 (2010).
19. B. Walsh, "Review of Tm and Ho materials; spectroscopy and lasers," Laser Phys. **19**(4), 855–866 (2009).
20. S. Lamrini, P. Koopmann, M. Schäfer, K. Scholle, and P. Fuhrberg, "Efficient high-power Ho:YAG laser directly in-band pumped by a GaSb-based laser diode stack at 1.9 μm," Appl. Phys. B **106**(2), 315–319 (2012).
21. M. Schellhorn and A. Hirth, "Modeling of intracavity-pumped quasi-three-level lasers," IEEE J. Quantum Electron. **38**(11), 1455–1464 (2002).
22. M. Digonnet, "Theory of superfluorescent fiber lasers," J. Lightwave Technol. **4**(11), 1631–1639 (1986).
23. J. Kwiatkowski, J. Jabczynski, L. Gorajek, W. Zendzian, H. Jelinkova, J. Sulc, M. Nemec, and P. Koranda, "Resonantly pumped tunable Ho:YAG laser," Laser Phys. Lett. **6**(7), 531–534 (2009).

1. Introduction

The solid state laser industry is moving towards smaller source crystal and higher power scaling capability and, rare-earth (Nd, Yb, Er) doped single crystal fibers (SCF) can potentially satisfy these requirements. With diameter of only 50-500 μm and length of tens of centimeters, SCFs have demonstrated being able to produce hundreds of watts of output power [1–5]. This is due to the fact that the thermal management relies on the larger surface-to- volume ratio (a characteristic unique to fiber architecture) compared to conventional bulk crystal. Apart from the above mentioned rare-earth dopants, Ho doped crystals operating in the eye-safe 2 μm spectral region are important for applications in medical surgery, atmospheric sensing and coherent radar [6]. The spectroscopy and laser performance of bulk Ho:YAG (both single crystal and ceramic) have been widely studied, but studies investigating SCF utilizing similar materials are relatively new.

In this paper, we investigated spectroscopic and gain properties of Ho:YAG SCF grown using the Laser Heated Pedestal Growth (LHPG) method. The large length-to-diameter ratio of the SCF samples assure multiple total internal reflection (TIR) bounces so the light guiding properties can be factored into the performance and differentiate from bulk material performance. The absorption and emission spectrum between the 1.9-2.1μm involving the $^5I_8$ and $^5I_7$ energy levels were measured and presented herein. In addition, using a Tm:fiber laser operating at 1932 nm for in-band pumping, the small signal gain was measured and the results are discussed using a first-order amplifier model for Ho:YAG.

2. Fabrication method for Holmium-doped YAG SC fibers

Table 1. Properties of glass, sapphire and YAG. T_p, melting temperature [12].

	Transmission Range (μm)	T_p (°C)	Thermal conductivity (W/m/K)	Young's Modulus (GPa)	Refractive index @1.06 μm
Silica glass	0.18-2.2	1000	1.38	73	1.45
Sapphire	0.17-5.5	2040	27.21	335	1.75
YAG	0.21-5.5	1940	14	300	1.81

SCFs have been grown since the early 1980s using variations of the LHPG technique with emphasize being on single crystal sapphire fiber for passive delivery of mid-IR laser radiation in the 2-5 μm [7–11]. Oxide crystals are mechanically and thermally more robust than glass fibers (see Table 1) [12]. In addition, unlike glass fibers, SCFs have a much higher spectral cutoff wavelength of ~3.5 μm making them attractive for MWIR applications. It is important to note that the SCFs grown are unclad in that there is no true fiber cladding as is the case with conventional glass core/clad fiber structures.

To fabricate 0.5% Ho:YAG SC fiber, the tip of a 1-mm-diameter 0.5% Ho:YAG source rod was melted using a CO_2 laser. Using an undoped YAG SC fiber as a seed source, the doped SCF was drawn at a rate of approximately 1mm/min. Figure 1 shows the schematic of LHPG setup along with detailed sketch of the molten zone. The source rod-to-fiber diameter reduction ratio was 3:1, thus the grown Ho:YAG SCF is approximately 330 μm in diameter. The fiber length is dependent upon the length of the source rod.

#209986 - $15.00 USD Received 11 Apr 2014; revised 3 Jun 2014; accepted 4 Jun 2014; published 10 Jun 2014

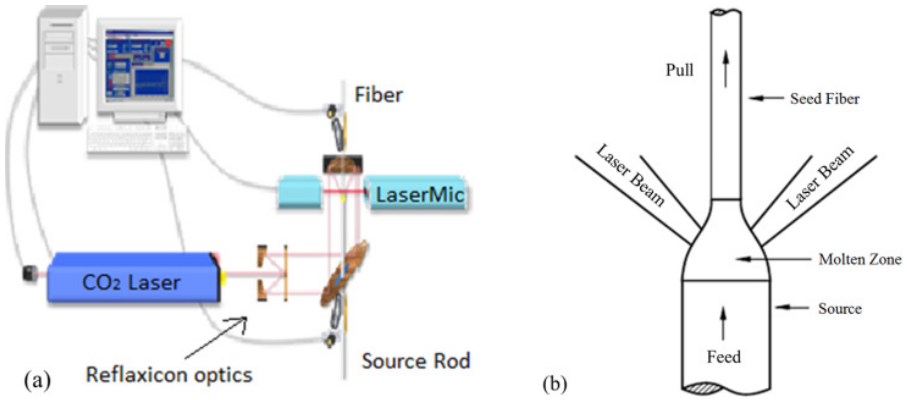

Fig. 1. (a) Overview of the LHPG apparatus, including CO_2 laser, reflaxicon optics, LaserMic, source rod, and fiber, and (b) Schematic diagram of the molten zone with CO2 laser beam contact at 360°.

It is difficult to achieve smooth surfaces and diameter control on SC fibers because the viscosity of the crystalline material is lower in the molten zone compared to the viscosity of glass. Thus, air Eddy currents, vibrations, motors steps, and laser-power variation lead to fluctuations in the drawn fiber diameter. To minimize the diameter variations, two feedback systems are employed. First, a standard proportional-integral-derivative (PID) controller provides feedback from the voltage supply, stabilizing the CO_2 laser power to ± 0.5%. Second, the laser micrometer displays the diameter at the frozen-molten interface and in this way feedbacks a signal to control the source and seed motors. In the present work, the diameter fluctuations across the length of the fiber were approximately ± 2%. For a more detailed description of the LHPG technique and feedback systems used for diameter control see [12].

3. Sample characterization

The overall cross-section of the SCF is slightly elliptical than circular, see Fig. 2(a). The cross sectional geometry is related to the orientation of the seed. Certain seed orientations result in different cross sections as shown previously [13]. A uniform CO_2 laser beam throughout the melting zone is very important for the symmetry of the SCF cross section. Figure 2(b) shows the side of the SCF and the shallow grooves with a period of ~10 μm distributed along the sidewall. The grooves are crystal facets associated with the orientation of the seed crystal. The maximum diameter change shown in Fig. 2(b) falls within ± 2% range.

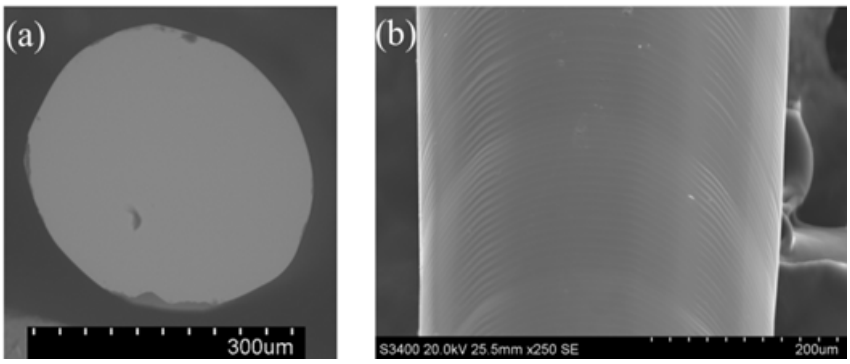

Fig. 2. (a) SEM image of the polished end-facet of the Ho:YAG SCF. (b) SEM image of the side of the sample showing the shallow grooves.

#209986 - $15.00 USD Received 11 Apr 2014; revised 3 Jun 2014; accepted 4 Jun 2014; published 10 Jun 2014

The $^5I_8 \rightarrow {}^5I_7$ absorption spectrum of the 0.5% Ho:YAG SCF sample was measured by a mid-infrared IPG tunable laser (Model HPTLM-Cr-ZnS/Se) using a resolution of 0.7 nm. A double-convex lens with a focal length of 75 mm was used to focus the laser beam into the SCF. In order to make sure the entire incident light can be coupled into the SCF, the radius of the laser beam was measured after the lens and plotted against the distance behind the lens as shown in the insert in Fig. 3. As the inset in Fig. 3 shows, the focused laser beam has a beam waist radius of 38 μm; such small beam waist guarantees that there will be multiple TIR bounces as the beam traverses the fiber. The first Ho:YAG SCF sample is 3.15 cm in length and both ends are polished. The proximal end of the fiber was positioned ~84 mm from the lens with the pump beam focusing just inside the fiber. The pump beam inside the SCF is guided by TIR. The power of the incident and transmitted beam were measured using a power meter (Ophir 30A-SH). The ratio of the transmitted and the incident power (taking into account the ~8.1% per surface Fresnel reflection losses) yields the attenuation coefficient including absorption and scattering loss. The measured attenuation coefficient is shown in Fig. 3.

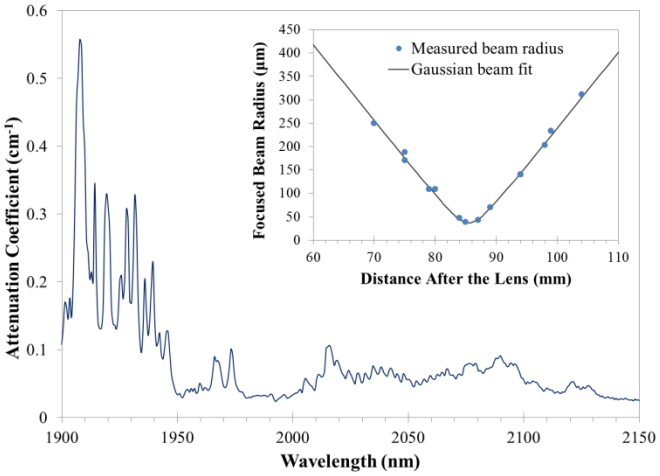

Fig. 3. The absorption spectrum of the Ho:YAG SCF. (Inset) The measured incident laser beam size with respect to the distance from the focusing lens.

The absorption spectrum shows the strongest absorption peak is at 1907.7 nm with a full width at half maximum (FWHM) of ~6 nm. Note that across the spectral region accessible with the tunable laser, the absorption spectrum has an average loss of 0.02 cm^{-1}, corresponding to a power loss of 6% along the 3.15 cm fiber length, which is probably due to scattering along the fiber as well as experimental error. This loss value is quite similar to Digonnet's measurement in [14], which shows the propagation loss increases with a decreasing fiber diameter. Cladding the SCF would obviously reduce the scattering loss.

The measured absorption spectrum is normalized and then used to calculate the absorption cross section σ_{abs} of the Ho:YAG using Eq. (1),

$$\sigma_{abs} = \frac{\alpha}{N}, \tag{1}$$

where α is the absorption coefficient and N is the doping concentration of Ho^{3+} ions, which is 6.5×10^{19} cm^{-3} for the 0.5% atomic doping concentration. According to McCumber theory, the emission cross-section can be obtained from the absorption cross-section line shape by using Eq. (2) [15,16],

#209986 - $15.00 USD Received 11 Apr 2014; revised 3 Jun 2014; accepted 4 Jun 2014; published 10 Jun 2014

$$\sigma_{emi} = \sigma_{abs} \frac{Z_{lower}}{Z_{upper}} \exp\left(\frac{h\nu_0 - h\nu}{kT}\right). \quad (2)$$

where Z_{lower} and Z_{upper} are the partition functions of the lowest sub-levels of the lower and upper states involved in this transition; ν_0 is the zero line frequency or the energy separation between the lowest sub-levels of the ${}^5I_8$ and ${}^5I_7$ levels in Ho^{3+} ions; h is Planck's constant; k is Boltzmann's constant and T is the room temperature. In our case, $Z_{lower}/Z_{upper} = 0.62$ [15]; ν_0 is 5227 cm^{-1} at room temperature [17], corresponding to 1913.1 nm in wavelength and T is 295 K. The calculated absorption (σ_{abs}) and emission (σ_{emi}) cross-sections as a function of wavelength are shown in Fig. 4. The peak emission in Ho:YAG occurs at 2090 nm. In comparison with bulk Ho:YAG data in [15,17], the measured σ_{abs} and σ_{emi} are about half of the bulk data, several reasons may contribute to this reduction in measurements. First, due to the segregation effect of the Ho ions, the SCF may contain fewer Ho ions than the source rod or their distribution [18]. The over-estimated Ho ion concentration will result in a lower cross section coefficient calculation. Second, the incident power level results in a 20% ~25% reduction in absorption due to the saturation effect. Improvements would be expected with lower incident power and increased sensitivity in the detector. Third, the spectral linewidth of the laser source will have a small impact on the measured absorption [17]. Since σ_{emi} is calculated from σ_{abs}, any small deviation in σ_{abs} will result in a significant difference in σ_{emi}.

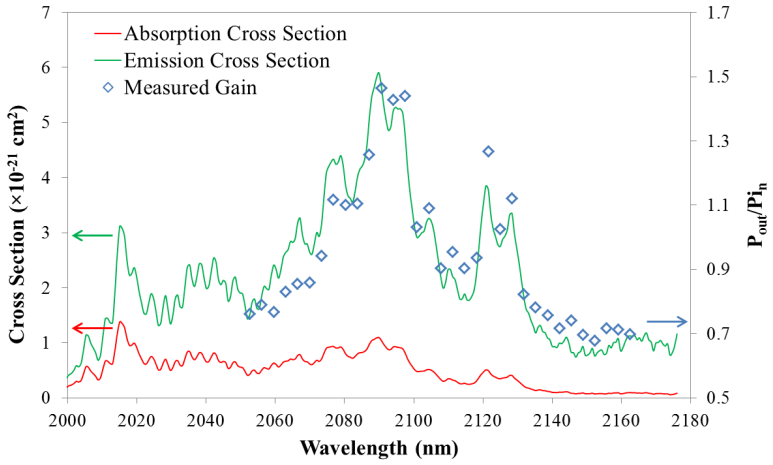

Fig. 4. The absorption (red) and emission (green) cross section of the Ho:YAG SCF. The emission cross section is calculated from the measured absorption spectrum using McCumber Theory. The blue markers are measured gain for different wavelengths; see detailed descriptions in section 5.

To verify the calculated emission cross section spectrum, the actual fluorescence emission spectrum from ${}^5I_7 \rightarrow {}^5I_8$ was recorded using the IPG tunable laser for in-band pumping. The pumping wavelength was 1932.2 nm, and this pumping wavelength was chosen as a trade-off between the absorption intensity and the available pump laser output power. Although the strongest absorption occurs at 1908 nm, the output power of the tunable laser at 1908 nm is less than half of the output power at 1932 nm. The SCF was pumped using the same setup as the absorption measurement. The 1932.2 nm pump light was coupled into the SCF from one end and the emissions were collected from the other end via a multi-mode fiber patch cord. The collected emissions were analyzed by a YOKOGAWA AQ6375 Optical Spectrum Analyzer (OSA). Figure 5 shows the emission spectrum under different pump power levels, and the emission peak is at 2090.6 nm, which is close to the calculated emission peak of 2090 nm. Comparing Fig. 4 and Fig. 5 it is clear that the calculated emission strongly correlates with the measurements.

#209986 - $15.00 USD Received 11 Apr 2014; revised 3 Jun 2014; accepted 4 Jun 2014; published 10 Jun 2014

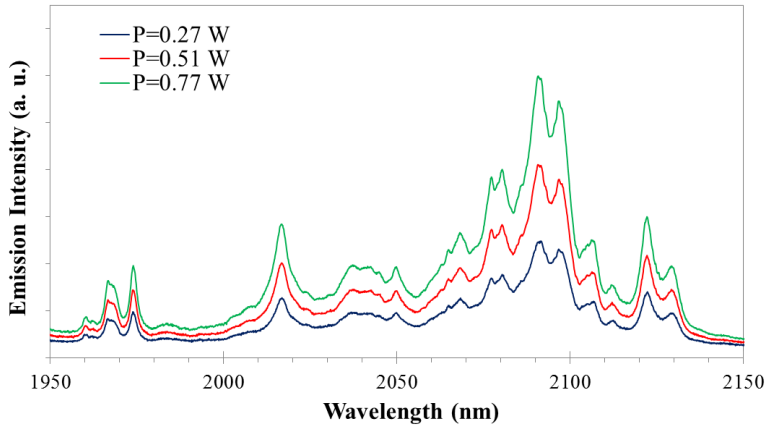

Fig. 5. The measured emission spectrum under different pump power using 1932.2 nm direct in-band pumping.

4. Small signal gain measurement and discussions

The small signal gain measurement setup is shown in Fig. 6. In order to demonstrate fiber like properties of the Ho:YAG SCF, a 400 μm diameter and 10.5 cm long 0.5% Ho:YAG SCF was grown. The fiber length-to-diameter ratio is ~250:1. The relative long length and small diameter provides a more fiber-like shape, therefore both pump and seed are guided in the SCF and the longer length insures that much more of the pump power is absorbed in a single pass for single pass gain measurements. The pump source is a 1932 nm Tm:fiber laser (modified from a Nufern Tm:fiber amplifier). The fiber laser provides a single mode output with maximum power of 7 W and spectral linewidth of 3 nm. The pump power was directed into the SCF using a broadband dichroic mirror reflecting nearly 100% of the pump beam while transmitting the seed signal wavelength. The counter-pumping amplification scheme was accomplished by coupling the seed into the SCF from the other end of the SCF. The output of a tunable IPG laser was coupled into a 9/125 single mode fiber (SMF) as seed delivering fiber to ensure the highest mode quality. Both seed and pump were single mode sources launched into the SCF, and both encounter multiple bounces within the SCF length as they propagate along the SCF. This architecture used in the current effort is in contrast to other SCF based amplification schemes, where only the pump is TIR guided in the SCF, while the seed encounters few, if any, TIR bounces in the SCF [5].

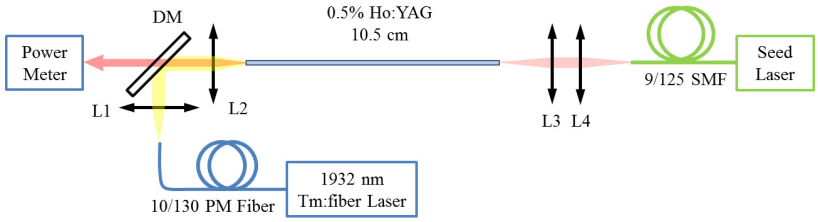

Fig. 6. Small signal gain measurement setup. DM, dichroic mirror, highly reflective at 1932 nm. L1, L2, L3, L4, collimating and focusing lenses. L1 is AR-coated and the losses of L2-L4 are taken into as well as the Fresnel reflection on both end-facets of the SCF.

Based on the intensity of the emission spectrum, a 2090 nm signal was chosen for measurement of the small signal gain. Three different incident powers of 87 mW, 225 mW and 380 mW were chosen to evaluate the gain as a function of pump power (see Fig. 7).

#209986 - $15.00 USD Received 11 Apr 2014; revised 3 Jun 2014; accepted 4 Jun 2014; published 10 Jun 2014

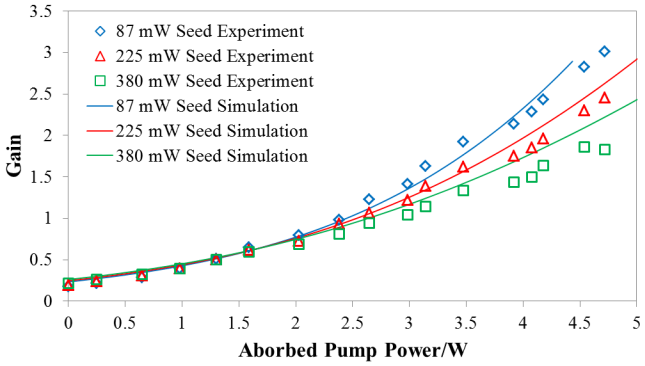

Fig. 7. Small signal gain with increasing pump power for three different seed power. Empty markers, experiment data. Colored lines, simulation curves.

Because of the quasi-four level nature of Ho:YAG, using the transition between ${}^5I_8$ and ${}^5I_7$ energy levels, the gain cross section is related to both absorption and emission cross sections by,

$$\sigma_g = \beta\sigma_{emi} - (1-\beta)\sigma_{abs} \tag{3}$$

where $\beta = N_2/N$ is the population inversion ratio [19,20], N is the doping concentration of Ho^{3+} ions, as mentioned above in section 3, is 6.5×10^{19} cm^{-3} and N_2 is the population in upper level. When there is no pump present, the transmitted seed is only 21% of the incident seed power due to absorption at the seed wavelength. With increasing absorbed pump power, the inversion ratio β (as well as σ_g) increases and the output seed power increases exponentially. At the point where $P_{out}/P_{in} = 1$, the SCF is not absorbing the seed anymore and the corresponding inversion ratio β is approximated as 14.5%. The pump power needed for compensating this seed absorption is approximately 2.5 W. For the same pump power, 87 mW seed experiences higher gain, which agrees with small signal gain and gain saturation effect, given by

$$g_{eff} = \frac{g_0}{1+\frac{P}{P_{sat}}} \tag{4}$$

where P_{sat} is the saturation power and $P_{sat} = AI_{sat}$. A is the mode area of the seed laser, which is approximated the cross section area of the SCF. I_{sat} is saturation intensity and,

$$I_{sat} = \frac{h\nu}{(\sigma_{emi}+\sigma_{abs})\tau} \tag{5}$$

where ν is the frequency of the seed wavelength and τ is the average lifetime of 8.5 ms for the upper ${}^5I_7$ level [21]. The seed laser with different power levels will have a different effective gain coefficient g_{eff}, which is related to the small signal gain coefficient g_0 by the ratio of seed power and saturation seed power. The higher the seed power, the smaller gain it will experience.

A simplified quasi-four-level rate equation based fiber amplifier model was adopted to simulate the small signal gain [21,22]. The results of the simulation are shown in Fig. 7. As can be seen, the simulated gain curves fit the measured data well when the pump power is relatively low. However the experimental and simulation results have some deviations as the pump power is increased. Several things can cause this. First, there is some spectral broadening and longitudinal mode competition of the Tm:fiber pump laser, which shifts the

#209986 - $15.00 USD Received 11 Apr 2014; revised 3 Jun 2014; accepted 4 Jun 2014; published 10 Jun 2014

pump slightly from the target spectral line of 1932 nm and reduces the absorption. Second, our measured emission and absorption cross section coefficients are impacted by scattering loss and saturation absorption, which can result in a slightly different saturation power, which impacts the calculated gain for seeds with different power levels. Third, scattering losses induced simulation deviation is relatively small when the gain is small, but quite noticeable in regions of high gain. Moreover, the simulations assumed a strong overlap of the pump and signal beams, which may not be the case for the multimode SCF section measured herein.

It is well known that bulk Ho:YAG has a relative broad emission band from 2050 – 2150 nm, and previous papers confirm the wavelength tuning capability of Ho:YAG solid state lasers [23]. Ho:YAG SCF shows the same broadband emission in this wavelength region, therefore it would be valuable to measure the gain at different wavelengths across this spectral band. In our case, the pump power was fixed at 3 W of absorbed pump power. The seed power level was also fixed while the seed wavelength was tuned across the spectral band, then the gain was measured and plotted as markers in Fig. 4 for the 10.5 cm piece, along with the measured emission and absorption cross section coefficients of the 3.15 cm piece for comparison. As we can see, the seed wavelength experiences the most gain and agrees with the peak emission wavelength at 2090 nm. It is worth mentioning that the gain at 2094 nm and 2121 nm is also substantial, which opens up the lasing and amplification at longer wavelengths if longer SCF length can be used for obtaining higher gain.

5. Conclusions

In summary, 0.5% Ho:YAG SCFs are fabricated using the LHPG method and tested in the fiber like regime with a length-to-diameter ratio of greater than 250:1. Although the diameter of the fiber shows some variations as well as some surface imperfections caused by fluctuations in fabrication parameters, such variations only effect the transmission by a small amount and the SCF fiber behaves as a fiber with multiple TIR bounces along its propagation path. The absorption and emission spectrum of the SCF together with the actual gain measurements verify that the SCF is a promising candidate for laser emission with efficient in-band pumping. In such cases, the high pump power needed for in-band pumping can be provided by Tm:fiber lasers which are commercially available.

The length of the SCF used in the gain measurement is 10.5 cm, and such a long length enables pumping of the SCF with a laser that matches the relatively weak absorption peak, e.g., in our case, 1932 nm, in lieu of the 1908 nm peak, which is the strongest absorption line. The advantage of choosing a weak absorption line is distributing the pump power more uniformly along the axis of the SCF, which reduces the thermal load, especially on the first few millimeters of the SCF. While the length we choose still maximizes total absorption of the pump. Efforts are underway to reduce the diameter and further limit the mode volume of the SCF. Additional work is also underway to model and understand the complex mode structure of the SCF and understand how this impacts the pump and signal beams in the SCF as well as constructing a SCF laser system. Meanwhile, fabrication of SCF with smaller diameters and various methods of cladding are currently under investigation for high power laser/amplifier applications. However, these results are strongly encouraging and additional measurements with increased pump power will further demonstrate the advantages of SCF over other bulk solid state systems for high power lasers in general.

Acknowledgments

Funding for this research was provided by the HEL-JTO through ARO W911NF-12-1-0536 and AFOSR FA9550-10-1-0543.